

Frequency Evolution of Neutron Peaks Below T_c : Commensurate and Incommensurate Structure in LaSrCuO and YBaCuO

Ying-Jer Kao

James Franck Institute, University of Chicago, Chicago, Illinois 60637, USA

Qimiao Si

Department of Physics, Rice University, Houston, TX 77251, USA

K. Levin

James Franck Institute, University of Chicago, Chicago, Illinois 60637, USA

(July 14, 2018)

We study the evolution of the neutron cross-section with variable frequency ω and fixed T below T_c in two different cuprate families. Our calculations, which predominantly probe the role of d -wave pairing, lead to generic features, independent of Fermi surface shapes. Among our findings, reasonably consistent with experiment, are (i) for ω near the gap energy Δ , both optimal LaSrCuO and slightly underdoped YBCO exhibit (comparably) incommensurate peaks (ii) peak sharpening below T_c is seen in LaSrCuO, (iii) quite generically, a frequency evolution from incommensurate to commensurate and then back to incommensurate structure is found with increasing ω . Due to their narrow ω regime of stability, commensurate peaks in LaSrCuO should be extremely difficult to observe.

PAC numbers: 74.25.Ha, 74.25.-q, 74.20.-z

The field of neutron scattering in high temperature superconductors has seen a variety of recent experimental discoveries associated with incommensurate and commensurate structure at $T < T_c$ [1–5]. These neutron data remain of central importance in the field of high T_c superconductivity: the combined momentum and frequency range covered by this technique is wider than that in virtually all other spectroscopies. It is mainly through this extended range that these neutron results have direct bearings on such important issues as dynamical stripes [6] and where the condensation energy comes from [7,8].

The goal of the present paper is to systematically address these observations over the *entire* momentum and frequency range that the experiments have covered, in the two different cuprate families (LaSrCuO and YBaCuO). In the process, we show that all of the above commensurate and incommensurate features are compatible with d -wave pairing superposed onto the normal state Fermi surfaces. In contrast to $T > T_c$, the details of the Fermi surface shape are of relatively less importance, and serve primarily to select out the ω regime where various commensurate or incommensurate features can be observed. The importance of the present work derives from the panoply of different experimental observations which are semi-quantitatively addressed here. These calculations have no adjustable parameters (besides those which were used originally [9,10] to fit some aspects of normal state data), so that their success or failure, upon comparison with experiment, should help select out viable theories of the cuprates.

Here, following previous work above [9] and below [10,11] T_c , we apply an RPA, three band scheme which we have developed to treat the effects of very strong Coulomb correlations [12]. It should be stressed that our RPA approach is not a weak coupling RPA. The Lindhard function χ_o used here is appropriate whenever the spin excitations are asso-

ciated with spin 1/2 and with an underlying Fermi surface—be it in a Fermi liquid [13–17], or in a spin-charge separated metal [18–20]. Our starting point is the dynamical susceptibility [12] $\chi(q, \omega) = \chi^o(q, \omega) / [1 + J(q)\chi^o(q, \omega)]$ where, at low T , the dominant contribution to the imaginary part of χ^o is given by

$$\text{Im}\chi^o(q, \omega) = \sum_k u(k, q)\delta(\omega - E_2(k, q)) \quad (1)$$

Here $u(k, q) = (1 - (\xi_k\xi_{k+q} + \Delta_k\Delta_{k+q})/E_kE_{k+q})$, and ξ_k represents the “bare” particle energy relative to the chemical potential while E_k is that of the superconducting quasiparticles. The important function $E_2(k, q) = E_k + E_{k+q}$ will play a key role in our analysis.

The RPA neutron cross section reflects a competition between effects associated with the Fermi surface shapes and pairing symmetry [via χ_o] and those from the residual exchange interaction [12] $J(q) = J_o[\cos q_x + \cos q_y]$, which derives from Cu–Cu interactions via the mediating oxygen band. While the YBaCuO system is a two layer material, our past experience [9,11] has shown that most of the peak structures associated with the neutron cross section are captured by an effective one layer band calculation, which we will investigate here. For definiteness, we have fixed the temperature at 4 K and assume the electronic excitation gap to be described by an ideal d -wave, $\Delta(q) = \Delta(\cos q_x + \cos q_y)$, where at $T = 4$ K, Δ is taken to be 17 meV in YBaCuO_{6.6} and 8 meV in optimally doped LaSrCuO. The breakdown of the Fermi liquid state is addressed only insofar as there may be precursor pairing or pseudogap effects, which lead to an excitation gap in the Lindhard function χ_o above T_c . Our calculations were based on a numerical procedure in which the Brillouin zone is subdivided into tetrahedral microzones [21]. Our peak heights are represented in arbitrary units, which are best quantified by

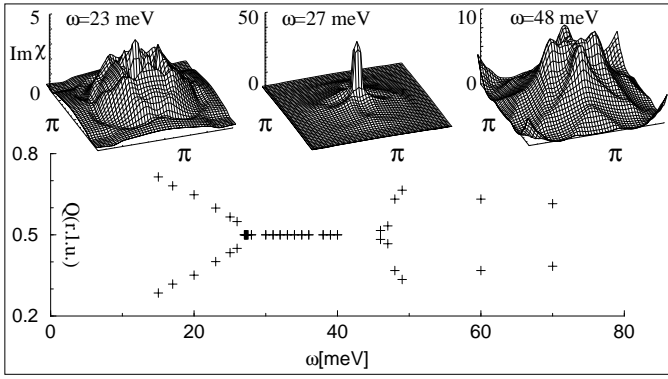


FIG. 1. Frequency evolution of neutron cross section ($Im\chi$) for $YBaCuO_{6.6}$. Units are arbitrary with corresponding normal state values given as a basis in text. Lower panel indicates the position of the dominant peaks in reciprocal-lattice units (r.l.u.).

noting that in the normal state, the peak values are around 2 for $LaSrCuO$ and for underdoped $YBaCuO$, whereas for the latter compound at optimal doping, the value is around 1. Presumably all peak structure with intensity less than this is not currently observable (since the normal state peak of $YBaCuO_7$ is essentially absent experimentally [22]).

In Figure 1 we show the evolution of the neutron peaks in underdoped $YBaCuO$ as a function of ω . These incommensurate peaks are first seen at $\omega \approx \Delta$; as frequency increases, the incommensurability is found to continuously decrease. This decrease is most apparent in the immediate vicinity of the onset of the resonance, [or (π, π) peak] which can be read off from the lower part of Figure 1, to be at around 27 meV, somewhat less than 2Δ . Just above resonance, the (π, π) peak becomes flat-topped possibly weakly incommensurate. It then broadens and remains structureless between 30-40 meV. Finally, above 45 meV, clear incommensurate structure re-appears. We find that our low ω incommensurate peak heights are in the ratio of about 1:10 when compared with the resonance feature. However, when the integrated spectral weight is considered, the ratio is about 1:2. Experimentally [1], the ratio of spectral weights is found to be 1: 3.8 .

The lower panel shows the detailed frequency evolution of the dominant peak position quantified as $(\pi, (1 \pm \delta)\pi) = (0.5, 0.5 \pm \delta/2) = (0.5, Q)$ in reciprocal-lattice units (r.l.u.). *The peaks evolve much as is seen experimentally* [2,3]. The primary difference between our observations and these particular experiments [2] is that over a range of frequencies, the incommensurate features coexist (although, not explicitly indicated in the lower panel) with the more dominant resonant peak. By contrast, experimentally, an energy scale E_c is associated with the frequency at which the various peaks merge. It should be stressed, however, that here we have not incorporated resolution limiting effects which may affect this detailed comparison between theory and experiment. A very early prediction for this lowest energy scale incommensurability was presented by our group in Ref. [10], where it was shown to be a consequence of d -wave pairing and relatively independent of the fermiology. Subsequent insights, using a related but

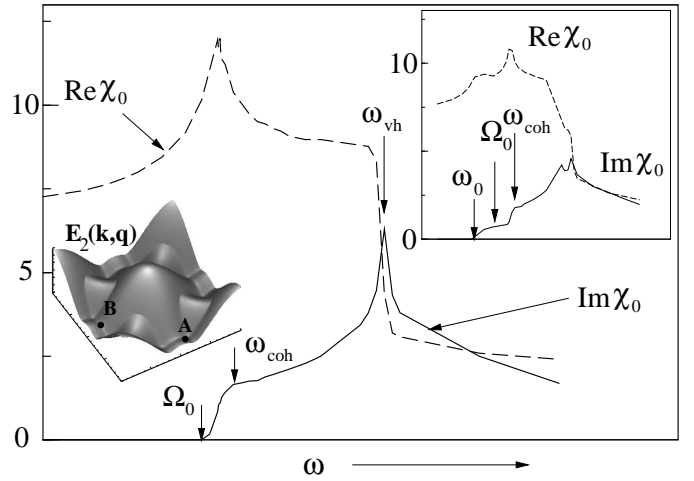


FIG. 2. Frequency dependence of $Im\chi_o$ and $Re\chi_o$ for $Q = (\pi, \pi)$. Upper inset is comparable plot for $Q = ((1 + \delta)\pi, \pi)$. The key characteristic energy scales (see text) are indicated. Lower (left) inset shows $E_2(k, q = Q_o)$; here A corresponds to the minimum of $E_2(k, q)$, (Ω_o) and B to the saddle point of $E_2(k, q)$, (ω_{vh}).

differently motivated formalism, were provided in Ref [19], which explicitly showed the influence of d -wave pairing on $Im\chi_o$.

To understand the origin of the various commensurate and incommensurate structures, in the main body of Figure 2 we plot the prototypical behavior of $Re\chi_o$ and $Im\chi_o$ for \mathbf{q} at the commensurate point $Q_o = (\pi, \pi)$; in the inset is shown the analogous plot for the incommensurate peaks. These plots, which were chosen to correspond to $YBaCuO$, contain, in effect, a summary of the key energy scales [23] which appear in $Im\chi_o$. Here we emphasize how they are reflected in $Re\chi_o$. These $Re\chi_o$ effects are essential because, through the RPA denominator they serve to greatly enhance a given characteristic feature in $Im\chi_o$. The four important energy scales which determine the behavior of $Im\chi$ (via simultaneous effects on $Im\chi_o$ and $Re\chi_o$) are given as (i) $\omega_o(\mathbf{q}) = \min E_2(k, q)$, (ii) ω_{vh} , the saddle point of $E_2(k, Q_o)$ (see point B in the inset), (iii) ω_{coh} the frequency where the rate of change of $u(k, q)$ drops abruptly. and, (iv) the onset for commensurate peaks $\Omega_o = \omega_o(Q_o)$ (see point A in the inset).

The related implications for $Re\chi_o$ are illustrated in Figure 2. The onset frequency Ω_o is accompanied by a substantial growth in $Re\chi_o$. However, once the frequency reaches the two-particle Van Hove energy ω_{vh} , determined by the saddle point shown as B in the inset, $Re\chi_o$ shuts down, as does the resonance. Figure 2, thus, shows that because of these $Re\chi_o$ amplifications along with the q -structure of $J(q)$, the commensurate peak will tend to dominate incommensurate structure in the range $\Omega_o < \omega < \omega_{vh}$, because of the small size of the RPA susceptibility which, in turn, yields a pole-like behavior in $Im\chi$. Incommensurate peaks only appear at the lower frequencies because their threshold ω_o is less than that of the commensurate structure. The appearance of incommensurability is associated with the d -wave state and is best seen pictorially in the upper right inset of Figure 3, shown for the

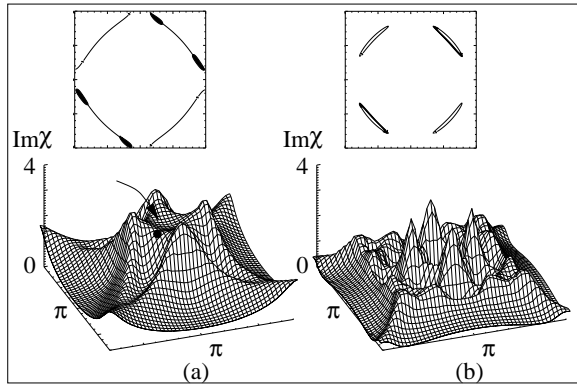


FIG. 3. Origin of peak sharpening in LaSrCuO below T_c . Superconducting and normal state processes contributing to cross section at indicated point are shown in right and left hand figures of upper panel, with line intensity corresponding to associated weight. Lower panels show the corresponding cross sections.

LaSrCuO family which contrasts nesting processes in the normal state (left) and d -wave superconducting state (right). Here the spectral weight of a given process is indicated by the intensity of the various lines. The magnitude of the incommensurability of the peak is determined by (i) energy conservation through the delta function in Eq. (1) along with (ii) coherence factor [$u(k, q)$] effects, which select out the most favorable regions from otherwise equivalent nesting vectors.

To summarize, we can consolidate our observations, along with a collection of some of the mechanisms [16,11,24] which have been proposed for the resonance in YBaCuO into a single inequality: low ω incommensurate peaks appear for $\omega_o < \omega < \Omega_o$, and commensurate peaks appear for $\Omega_o < \omega < \omega_{vh}$. At still higher frequencies the peaks are again incommensurate. Ω_o is always somewhat less than 2Δ because of the nodal structure of the d -wave gap.

Indeed, the results of Figure 2 are rather generic and can be used to address the LaSrCuO family as well, where unusual incommensurate structures in the cross section have been experimentally reported [4] below T_c for a range of low ω , above Δ . These, and related “spin gap” features have not yet been addressed theoretically. Here, we demonstrate that, in contrast to Ref. [25], these features— which are closely connected to the (low energy scale) incommensurate peaks discussed above for YBaCuO— are unrelated to fermiology effects and to presumed “incommensurate spin structure”. They depend exclusively on the d -wave pairing symmetry. Figure 3 shows a comparison of the cross section in the normal (left) and superconducting (right) phases of optimally doped LaSrCuO at low ω . The peak sharpening below T_c was first observed experimentally [4]. Its origin can be traced to the differences (above and below T_c) in the initial and final scattering processes along constant energy contours, which contribute to $Im\chi^o$ at a given point. These processes are shown in the upper panels of Figure 3 for a particular point \mathbf{q} indicated on the normal state cross section. It can be seen that in the superconducting phase, as a consequence of the opening of the gap, there is relatively little weight at the \mathbf{q} point in question,

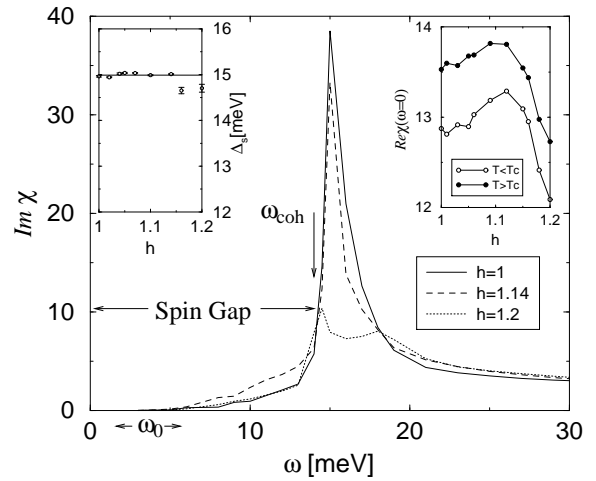


FIG. 4. $Im\chi$ for LaSrCuO in the superconducting state along $\mathbf{q} = (0.56h, 0.44h)(r.l.u.)$ at $h = 1, 1.14, 1.2$. Lefthand inset shows the “spin gap” obtained by fitting $Im\chi$ to a Lorentzian. Right-hand inset compares $Re\chi$ at $\omega = 0$ in the normal and superconducting states.

thereby leading to a greatly reduced scattering in the region *between* the incommensurate peaks below T_c .

In order to gain more experimental insight into the behavior of the neutron peaks of LaSrCuO in the superconducting phase, the authors of Ref. [4] measured $Re\chi$ at low frequencies and at the incommensurate points. They also addressed the details in the frequency onset of the cross section, measured via $Im\chi$, for a range of different wave-vectors. To determine $Re\chi$, the cross section was fitted to a simple Lorentzian-like form [4] peaked at Δ_s . Here, we use the directly calculated $Re\chi$ to extract Δ_s . The resulting experimental curves look qualitatively similar to the theoretical plots shown in the right hand inset of Figure 4. A reduction in $Re\chi(\omega = 0)$ between the normal and superconducting phase can be associated (via general Kramers Kronig relations) with a low ω suppression in the spectral weight of $Im\chi$. In the present theoretical scheme, this suppression derives from the opening of a d -wave superconducting gap. It is important, however, to stress that the d -wave symmetry in $Im\chi$ is not immediately evident from either the plots in Figure 4 or the data. Indeed, the main portion of the figure shows $Im\chi$ vs ω for three different values of the incommensurate wave-vector $\mathbf{q} = (1.12h\pi, 0.88h\pi) = (0.56h, 0.44h)$ (r.l.u.), and indicates that the onset frequency in $Im\chi$ is relatively constant in \mathbf{q} . This onset frequency or “spin gap” Δ_s , is plotted more completely for a range of wave-vectors in the upper left inset. Here the range is taken to coincide with its experimental counterpart and the results shown compare favorably with experimental data from Ref. [4]. While the calculated spin gap magnitude is larger by a factor of 2 than experiment, it should be stressed that the downturn at large h is seen experimentally, and is predicted to be systematic.

Why then is there no d -wave signature in the spin gap frequency? This follows because the \mathbf{q} structure associated with the d -wave gap appears inside the integral over \mathbf{k} in the Lind-

hard function χ_o . Moreover, the \mathbf{q} points chosen in the main body of the figure and in the left hand inset, while consistent with those measured in Ref. [4], do not reflect most directly the superconducting gap. In our calculations the spin gap Δ_s is found to be associated with the coherence (coh) factor energy scale, ω_{coh} , which is relatively wave-vector independent in the region studied. However, it is the slightly lower, threshold frequency at which $Im\chi$ first becomes non-zero ($\omega_o(q)$), which most closely reflects Δ_q . (Indeed, ω_o varies by a factor of 2 for the q values indicated). By contrast with ω_{coh} , at ω_o , the cross section has relatively little detectable weight.

What, then, are the similarities between the LaSrCuO and YBaCuO families? There are claims in the literature [1,4] that the incommensurabilities for near-optimal LaSrCuO and for YBaCuO_{6.6} are the same, as are the spectral weights once ω is scaled by the appropriate T_c . To address these more quantitative issues we first note that the $\omega = 23$ meV incommensurability shown in underdoped in YBaCuO in Figure 1 is comparable, ≈ 0.1 (r.l.u.), to that plotted in Figure 3 for optimal LaSrCuO.

Moreover, as an estimate of the q -integrated spectral weight, we find that the Brillouin zone averages, called $\langle Im\chi(\mathbf{q}, \omega) \rangle_{BZ}$ are equal for YBaCuO_{6.6} and optimal LaSrCuO at 22 meV and 13 meV, respectively. If we rescale ω by T_c in each case ($T_c \approx 60$ K for YBaCuO_{6.6} [26], 35 K for La_{0.85}Sr_{0.15}CuO₄ [27]), it follows that at about the same rescaled frequencies, these intensities are nearly equal. It should be stressed that we regard the underlying physical origin of the incommensurate peaks in the superconducting state of the two cuprates to be the same (as discussed in the context of Figure 2), but that the characteristic energy and wave-vector scales need not be precisely equal. Indeed, the incommensurability is now found to be ω dependent [2], which makes the numerical comparisons somewhat less meaningful. Finally, it should be noted that the main body of Figure 4 is rather generic (as seen in Figure 2). These plots of $Im\chi$ together with their normal state counterparts, are in reasonable agreement with the results of Ref. [4].

What then is the most significant difference between the LaSrCuO and YBaCuO families? We find that this difference derives from the fine details of the bandstructure which are then reflected in the range of stability of commensurate peaks. The former compound is presumed to have a significantly smaller next nearest neighbor hopping integral (t') so that the two particle Van Hove feature [16,11] ω_{vh} appears much closer to Ω_o . Indeed, for LaSrCuO essentially all energy scales (for commensurate structure) are compressed down to Ω_o . In this way there is a much smaller frequency window (≈ 2 meV) for commensurate peaks in the LaSrCuO family than in its YBaCuO counterpart. Thus far, searches within the broader 5 meV interval have failed to see them. While this narrow regime of stability will make them difficult to see, commensurate peaks appear to be a fairly general feature of the RPA-like d -wave approach to the neutron cross section.

In summary, it should be stressed that the frequency evolution from incommensurate to commensurate and then to incommensurate peaks in the neutron cross section (as shown by the lower panel in Figure 1) is a generic feature of the present

approach, and because it appears to be observed experimentally in at least two cuprate families [1,5], it will be important to establish whether an alternative scheme, such as the ‘‘stripe’’ picture can lead to similar behavior.

We would like to thank G. Aeppli for informative and illuminating discussions. This work was supported by the NSF under awards No. DMR-91-20000 (through STCS), and No. DMR-9808595 (through MRSEC). Q. S. is supported in part by NSF Grant No. DMR-9712626, Research Corporation, and A. P. Sloan Foundation.

-
- [1] H. A. Mook *et al.*, Nature **395**, 395 (1998).
 - [2] M. Arai *et al.*, Phys. Rev. Lett. **83**, 608 (1999).
 - [3] H. F. Hong *et al.*, cond-mat/9910041 (unpublished).
 - [4] B. Lake *et al.*, Nature **400**, 43 (1999).
 - [5] H. A. Mook *et al.*, cond-mat/9811100 (unpublished) and private communication.
 - [6] V. J. Emery and S. A. Kivelson, cond-mat/9809083 (to be published in J. of Supercond.).
 - [7] E. Demler and S.-C. Zhang, Phys. Rev. Lett. **75**, 4126 (1995).
 - [8] E. Demler and S.-C. Zhang, Nature **396**, 733 (1998).
 - [9] Q. M. Si, Y. Y. Zha, K. Levin, and J. P. Lu, Phys. Rev. B **47**, 9055 (1993). In LaSrCuO, $\epsilon_p - \epsilon_d^0 = 4$ eV, $V_{pd} = 0.6$ eV, and $t_{pp} = -0.15$ eV; in YBCO_{6.6}, $\epsilon_p - \epsilon_d^0 = 5$ eV, $V_{pd} = 1.29$ eV, $t_{pp} = 1.2$ eV, and $t'_{pp} = -1.0$ eV.
 - [10] Y. Zha, K. Levin, and Q. M. Si, Phys. Rev. B **47**, 9124 (1993).
 - [11] D. Z. Liu, Y. Zha, and K. Levin, Phys. Rev. Lett. **75**, 4130 (1995).
 - [12] Q. Si *et al.*, Physica C **162-164**, 1467 (1989).
 - [13] P. B. Littlewood *et al.*, Phys. Rev. B **48**, 487 (1993).
 - [14] P. Benard, L. Chen, and M.-M. S. Tremblay, Phys. Rev. B **47**, 15217 (1992).
 - [15] N. Bulut and D. J. Scalapino, Phys. Rev. B **53**, 5149 (1996).
 - [16] I. I. Mazin and V. M. Yakovenko, Phys. Rev. Lett. **75**, 4134 (1995).
 - [17] N. Bulut and D. J. Scalapino, Phys. Rev. B **50**, 16078 (1994).
 - [18] T. Tanamoto, H. Kohno, and H. Fukuyama, J. Phys. Soc. Japan **61**, 1886 (1992).
 - [19] J. Brinckmann and P. A. Lee, Phys. Rev. Lett. **82**, 2915 (1999); Related calculations were independently reported by Qimiao Si and K. Levin (unpublished, 1998).
 - [20] L. Yin, S. Chakravarty, and P. W. Anderson, Phys. Rev. Lett. **78**, 3559 (1997).
 - [21] J. Rath *et al.*, Phys. Rev. B **11**, 2109 (1975).
 - [22] H. Fong *et al.*, cond-mat/9902262 (unpublished).
 - [23] M. Lavagna and G. Stemann, Phys. Rev. B **49**, 4235 (1994).
 - [24] H. F. Fong *et al.*, Phys. Rev. Lett. **75**, 316 (1995).
 - [25] D. Morr and D. Pines, cond-mat/9807214 (unpublished).
 - [26] P. Dai, H. A. Mook, and F. Doğan, Phys. Rev. Lett. **80**, 1738 (1998).
 - [27] K. Yamada *et al.*, Phys. Rev. Lett. **75**, 1626 (1995).